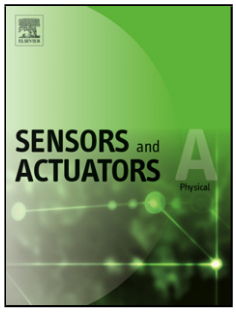

Title: A Precise Embedded Curvature Sensor Module for Soft-Bodied Robots

Author: Selim Ozel Nehir A. Keskin Darien Khea Cagdas D. Onal

PII: S0924-4247(15)30158-8
DOI: http://dx.doi.org/doi:10.1016/j.sna.2015.09.041
Reference: SNA 9336

To appear in: *Sensors and Actuators A*

Received date: 19-12-2014
Revised date: 28-9-2015
Accepted date: 30-9-2015

Please cite this article as: Selim Ozel, Nehir A. Keskin, Darien Khea, Cagdas D. Onal, A Precise Embedded Curvature Sensor Module for Soft-Bodied Robots, *Sensors & Actuators: A. Physical* (2015), http://dx.doi.org/10.1016/j.sna.2015.09.041

A Precise Embedded Curvature Sensor Module for Soft-Bodied Robots

Selim Ozel, Nehir A. Keskin, Darien Khea, and Cagdas D. Onal

Abstract

As an emerging field, soft-bodied robots require profoundly different approaches to sensing and actuation compared to their rigid-bodied counterparts. Electro-mechanical design, fabrication, and operational challenges due to material elasticity significantly complicate embedded, modular and precise proprioceptive feedback. This work presents a novel curvature sensor module to address the unique soft robotic specifications. The proposed device utilizes a magnet and an electronic Hall effect sensing component to accurately measure curvatures on a soft-bodied bending segment on a flexible circuit board, ensuring contact-free sensing. We verify performance of sensor modules on static and dynamic bending deformations based on a single initial calibration step. To the best of our knowledge, the presented device is the first modular and integrated soft-bodied sensor design that is demonstrated to be accurate up to 7.5 Hz with a root mean square error of 0.023 cm^{-1} between measured and actual curvature without filtering out the intrinsic noise, and available for use with soft-bodied kinematic bending chains.

Keywords: Soft robots, Curvature Sensor, Hall Effect

1. Introduction

Obtaining kinematic configuration information of soft bodied robots is one of the current challenges in the field. The traditional approach to determine the configuration of a rigid kinematic chain is to obtain discrete angle measurements from each joint. In contrast, soft bodied robots possess infinitely many passive degrees of freedom [1, 2] as a result of continuously deformable segmented bodies [3, 4], emphasizing the need for new sensing techniques. Our research problem in this paper is to explore the capabilities

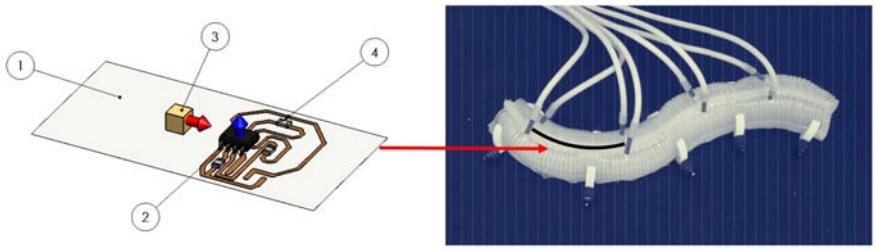

Figure 1: Left: Computer Aided Design of the sensor assembly is shown. Number definitions: 1) Flexible substrate, 2) Hall effect IC, 3) Magnet, 4) Circuit paths and components. Red and blue arrows indicate horizontal (x-axis) and vertical (y-axis) directions respectively. Right: The sensor is built to be integrated in the middle of the soft snake robot for proprioceptive curvature measurements.

of a novel embedded soft curvature sensor designed to capture configuration information from soft robotic bending segments.

The emerging field of soft robotics suffers from a lack of modeling and control efforts for both kinematic configuration and dynamic properties. We believe soft manipulators and soft-bodied mobile robots [5, 6, 7, 8, 9] can expand their capabilities through accurate models, and corresponding feedback controllers. Our approach to modeling the configuration of a soft robot is based on defining the bending deformation of soft segments as curvatures [4, 10, 11] instead of discrete angles. Thus, the orientation and position of every point on a continuously deformable segment is uniquely defined with respect to its curvature. Robot configuration is then modeled as a kinematic chain of segments, where each segment is defined by a single curvature value. In prior work, we were able to model and reproduce lateral undulation for a soft robotic snake comprising four soft bidirectional bending segments [4, 10]. This approach requires us to sensorize a soft body for implementation and this is the main motivation behind our curvature sensors.

This work details the design, fabrication, and experimental verification of a soft curvature sensor comprising a miniature magnet and a Hall effect measurement integrated circuit (IC). The magnet is positioned in a specific way with respect to the Hall element on a flexible circuit (see Figure 1) to measure the curvature of bidirectional out-of-plane deformations in a standalone package, without the need for external electronics. This is a versatile approach, which can be adapted to measure other physical deformations in a soft body. For example, a setup consisting of a magnet mounted over a Hall

Effect sensing component can be used for measuring normal forces. In this work, we are limiting our attention to curvature sensing due to its practical applications on our soft robotic snake [10, 12].

Hall elements are compact, accessible, and inexpensive. The quick response and accuracy of Hall elements for traditional robotic applications have previously been verified for joint angle proprioception [13, 14] as well as tactile exteroception [15, 16]. Contact-free sensing capabilities are highly desired for soft robotic research [17]. Thus, a unique advantage of our non-contact magnetic field measurement approach, is its negligible effect on material stiffness.

Alternative solutions to curvature sensing include commercial resistive flex sensors, optical fiber Bragg gratings, and embedded liquid metals. Resistive flex sensors offer a simple and compact solution for embedded sensing in soft robotics. Nevertheless, we concluded in a preliminary study (reported elsewhere) that they suffer from dynamic artifacts, such as delayed response and drift.

Optical fiber Bragg grating is a powerful sensing solution for deformable bodies used successfully for force measurements on a soft finger [18], and shape reconstruction [19]. Although this technology facilitates highly accurate curvature measurements using a thin and flexible optical fiber, the required supporting hardware disables embedded operation, especially for tetherless mobile robots with many degrees of freedom.

A novel and specialized sensor technology for soft robots is the use of liquid metals embedded in rubbers, a technology stemming from mercury-in-rubber strain gauges from 1960s [20]. Thus, dimensional changes due to deformations in the substrate are reflected as resistance changes by the liquid metal. Recent work incorporates fluidic channels inside silicone rubber filled with eutectic Gallium-Indium (eGaIn) to measure joint angles of a finger [21] and for a tactile sensing array [22]. A short survey on sensors built with eGaIn is given in [23]. An interesting work that applies eGaIn sensors to a suit for gait detection is presented in [24]. Main limitation of eGaIn sensor is a relatively complicated fabrication phase. They require a 3D mold with channels. Afterwards eGaIn is injected from one side of the mold while air inside the channels is vacuumed from the other side. Thus, repeatability and complexity in manufacturing these sensors may be a challenge.

To address the fundamental challenge of providing accurate and dynamic proprioceptive feedback for soft-bodied robots, this work proposes a novel soft curvature sensor, based on the state of the art in flexible sensing technologies.

Specific contributions of this work are as follows:

- Robust and precise curvature feedback with rapid response for soft-bodied robots.
- Integrated measurement of kinematic configuration for soft-bodied arms and mobile robots composed of soft bending segments.
- A custom test platform for soft-bodied curvature sensors.

The following section explains the fundamentals of design, modeling, and fabrication. We provide detailed information on positioning of the magnet-sensor pair, design specifications, and manufacturing steps. We present results of numerically simulating the sensor response to different curvatures. Simulation results inform the positioning of discrete elements, gain and offset adjustment. We also present a test platform to repeatably characterize and verify our soft curvature sensors under static and dynamic loading conditions. Section 3 displays and discusses results obtained from the proposed curvature sensor using the custom test platform, reporting experimental results on calibration, repeatability, as well as static and dynamic verification of the proposed soft curvature sensors.

2. Methods

2.1. Curvature Sensor Design

The main requirements for a curvature sensor for soft robotics are flexibility and minimal effect to material stiffness. Along with structural specifications, accurate, precise and fast responses are also required for feedback control applications based on proprioceptive curvature sensing.

We adopt locomotion parameters of a soft-bodied snake robot [4] as another set of design specifications to achieve an embedded curvature sensing module that is consistent and compatible with the literature. The soft robotic snake deforms between 0.2 cm^{-1} and 0.4 cm^{-1} and the frequency of traveling curvature waves to achieve undulatory locomotion is between around 2 Hz. Thus, a curvature sensor working at frequencies above around 3 Hz without dynamic attenuation is expected to provide accurate reconstruction of the robot configuration.

An accurate mapping is required to convert measurements to curvature values. Two desired properties of the calibration function are linearity and injectivity. To show that such a mapping exists, we developed a simulation

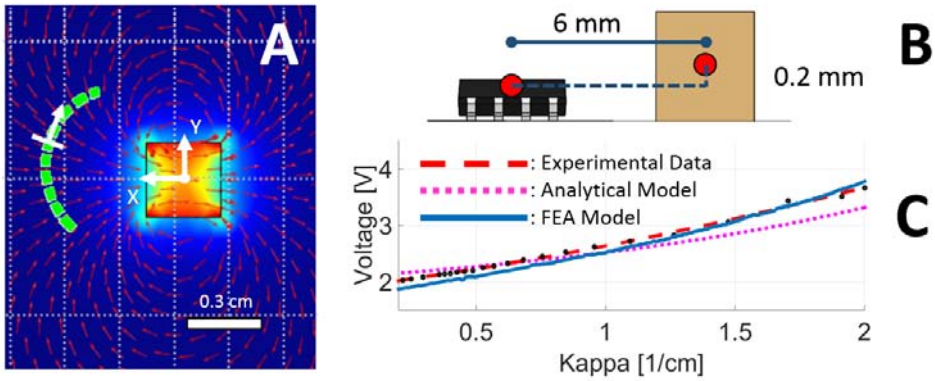

Figure 2: (A) FEA data obtained from a simulation of sensor motion. The dashed green curve is the trajectory of the sensor from -1.5 cm^{-1} to 1.5 cm^{-1}. Arrow indicates the sensing direction that is always tangential to the trajectory. An inherent offset due to vertical level difference between magnet and sensing surface can also be observed from the mid-point of the trajectory. (B) shows the vertical and horizontal offset between the magnet and the sensor. (C) Sensed magnetic flux density vector magnitude was computed between 0.5 cm^{-1} and 2.0 cm^{-1}. The dashed red curve is a least squares fit obtained from voltage measurements from 30 different curvatures. The solid blue curve is the voltage versus curvature result from the FEA simulation. The dotted purple curve is the simulation result obtained from the theoretical model between 0.5 cm^{-1} and 2.0 cm^{-1}. Both in simulations and in the application, we use a cube magnet with a side length of 3 mm. The magnetization value for simulations is 8.0x10^5 A/m.

platform that considers both finite element analysis of a magnet and its theoretical model. Once the sensor is calibrated and a mapping is obtained, curvature measurements are absolute (i.e. not subject to initial conditions or temporal variations).

Theoretical modeling of magnetic flux density vectors around a magnet provides intuition on the curvature sensor response. A simple dipole model of magnetism approximates these vectors, but it does not include volumetric constraints. A more accurate 2-D analytical model of a rectangular magnet is derived in [25]. According to this model, the Cartesian magnetic field vector components in the magnet frame can be written as:

$$B_x(x,y) = \frac{\mu_0 M_s}{2\pi}\left(\arctan\frac{2h(x+w)}{(x+w)^2+y^2-h^2} - \arctan\frac{2h(x-w)}{(x-w)^2+y^2-h^2}\right), \quad (1)$$

$$B_y(x,y) = \frac{\mu_0 M_s}{4\pi}\left(\ln\frac{(x+w)^2+(y-h)^2}{(x+w)^2+(y+h)^2} - \ln\frac{(x-w)^2+(y-h)^2}{(x-w)^2+(y+h)^2}\right). \quad (2)$$

In the equations above, B_x and B_y are magnetic flux density vector components in different (x, y) positions with respect to the magnet. The coordinates and the origin of the frame, in which equations are defined, can be seen in Figure 2. X-axis and Y-axis are parallel to horizontal and vertical lines respectively, and origin of the magnet frame is attached to the middle of the cube magnet. μ_0 is the relative magnetic permeability of the medium. M_x is the surface magnetization magnitude of the magnet. Finally, h and w are the height and width of the rectangular magnet.

To maximize accuracy, we used the magnetic flux density vector data obtained from finite element analysis (FEA), using the COMSOL package, to develop a kinematic simulation within the working range of the sensor. COMSOL allows users to model magnets with respect to remnant magnetic induction. Also, it is trivial to get a 3D surface with magnetic flux density vectors around the magnet. Figure 2 displays magnetic field density vectors around a magnet along with the trajectory covered by the Hall element during the simulation. The design space of this sensing approach comprises multiple parameters such as: magnet size and orientation, distance between the sensor and the magnet, and the sensitivity of the Hall element. For example, if the magnetization axis of the magnet is not perpendicular to sensing direction, the mapping from voltage to curvature would not be bi-directional. This numerical approach provided us with rapid evaluation of all design parameters to serve as preliminary values for fabrication.

We exported the FEA data to MATLAB as a lookup table for magnetic flux density vectors at different positions around the magnet. The position of the Hall element with respect to magnet is a function of curvature expressed as:

$$\begin{aligned} x &= \frac{1}{\kappa}\sin(\kappa s), \\ y &= \frac{1}{\kappa}(1-\cos(\kappa s)), \end{aligned} \quad (3)$$

where x and y are positions along the length of the segment, κ is the curvature of the segment in cm^{-1} units, s is the normalized arc-length, $s \in [0, 1]$ [10]. x and y positions are defined in the magnet frame and axis representations can be seen in Figure 2. The Hall element measures the magnetic flux density

vector component in the perpendicular direction to its surface, which is taken into account in the both analytical calculations and numerical simulations.

Figure 2 displays simulated magnetic flux density vector magnitude on the Hall element for curvature values between 0.2 cm^{-1} and 2 cm^{-1}. The horizontal distance between magnet and sensor in this simulation was 6 mm and the vertical distance was 0.2 mm. Horizontal and vertical distance definitions can also be seen in Figure 2. Results from this simulation suggests that there exists a one-to-one, nearly linear mapping between the measured component of the magnetic field vector and curvature.

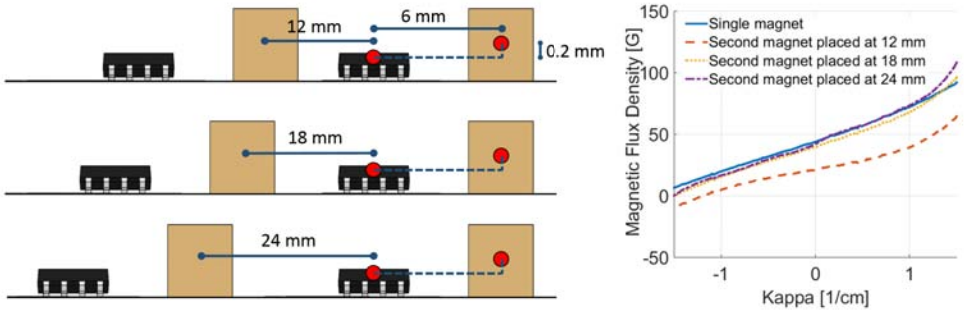

Figure 3: A second magnet is placed at distances 12, 18, and 24 mm near the Hall element to analyze the effects of a cascaded sensor system. Results suggest that another sensor pair can be placed at 18 mm, and it will not create significant interference in the sensed magnetic flux density. The sketch on the left is not to scale.

Sensitivity and offset of the magnetic field measurement circuitry depends on positioning of the magnet, as well as the vertical distance between the magnet and the Hall element. Simulation results suggest that the sensitivity of magnetic field measurement to be around 40 mV/G, to utilize 70 % voltage range between $0 - 5$ V in positive and negative directions. Due to directional bias, a voltage offset of 0.35 V was added to achieve bi-directional measurement without saturation.

We also looked into effects of crosstalk between other sensors or ferromagnetic materials in the environment inside our simulation. We placed another magnet at three different distances in the horizontal direction and observed their effect on the Hall element. The horizontal distance between the surface layer and the magnet is 6 mm. Through simulations, we discovered that crosstalk between sensors may become an issue when another sensor is

placed between 12-18 mm. We also discovered that crosstalk has an effect on measured data in high curvature values around -1.5 cm^{-1} and 1.5 cm^{-1}. Results can be seen in Figure 3.

2.2. Manufacturing

Manufacturing of the curvature sensor is composed of two stages: printing electronics and molding silicone rubber. Electronic circuitry is printed on two substrates, copper-clad FR4 and copper-foil laminated polyester (PET), using a standard solid-ink printer. The flexible substrate is then etched to obtain circuit traces and discrete components are populated manually to result in a fully custom-printed flexible circuit. The Hall Effect IC is AD22151. A B222G-N52 magnet is bonded to the etched sheet at the desired location based on our simulation results.

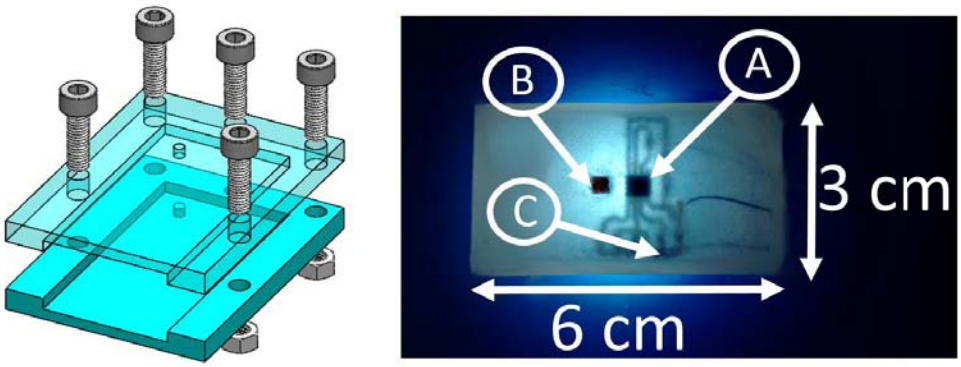

Figure 4: Left: Isometric view of the mold is shown. Silicone rubber is poured into the inner chamber from the open space that can be seen in front and isometric views. The length, width and thickness of the inner chamber are 60 mm, 30 mm and 5.6 mm respectively. The length, width and thickness of the overall mold are 50 mm, 70 mm and 11 mm, respectively. Right: A curvature sensor prototype is shown. The Hall effect IC (A), the magnet (B), and circuit traces (C) can be seen in the figure. A flexible circuit layer is positioned in the middle of the silicone layer. The Hall effect IC has an internal op-amp for offset and sensitivity adjustments. Circuitry and resistances are also embedded inside the silicone. The total thickness of the sensor is 7 mm.

For greater compatibility with bending type soft actuators, the curvature sensor circuit is embedded inside EcoFlex 0030 silicone rubber from Smooth-On. 3-D printed mold design for the sensor is shown in Figure 4. Screws passing through the flexible sheet and two pieces of the mold guarantee flat

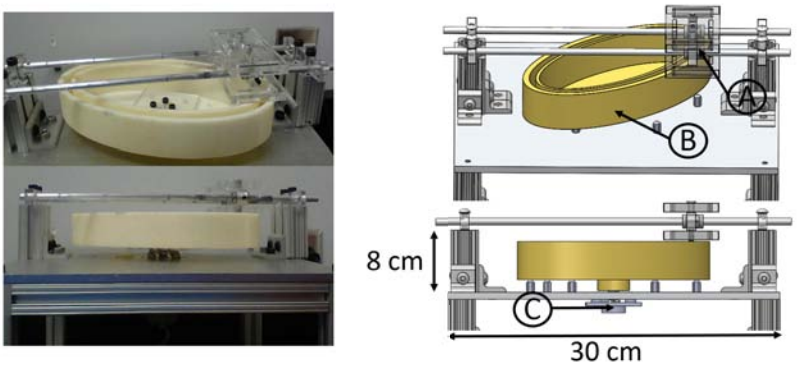

Figure 5: Left Panel: Actual test platform with the ellipse track is shown. Right Panel: CAD models of the platform are shown. (A) is the mounting platform for the sensor. It can move in a single direction along the aluminum rods. The connection is made with linear bearings to reduce friction. There is a rod coming down from the platform that is attached to the sensor. This rod pulls the sensor inside the track as the motor turns it. (B) 3D printed elliptical track. (C) A motor is mounted below the square shaped aluminum platform and it is coupled to the 3D printed track. The edge length of the platform is 30 cm. The thickness of the elliptical track is 4.5 cm including the motor coupling.

mounting. Silicone rubber is then introduced inside the mold and cured at 60 °C for 40 minutes. The curing operation finalizes the manufacturing of the sensor. An example of the soft sensor segment can be seen in Figure 4.

Provided with electronic components, circuit design, and molds; overall manufacturing time to build the sensor from scratch is approximately two hours. Printing circuit traces and etching takes 30 minutes. Components can be manually soldered in under 15 minutes and curing silicone rubber takes around 40 minutes. Note that all these processes can be automated and performed in parallel to speed up the manufacturing process for larger volumes.

2.3. Test Platform

Deforming a silicone rubber segment into known curvatures, repeatedly and precisely is not a trivial task. One way to achieve it is to attach soft bending actuators powered by pressure to the sensor segment, and actuate it with different pressure values. Details of such actuators can be found in [26]. The deformation could be tracked with a visual system to compute the curvature of the segment.

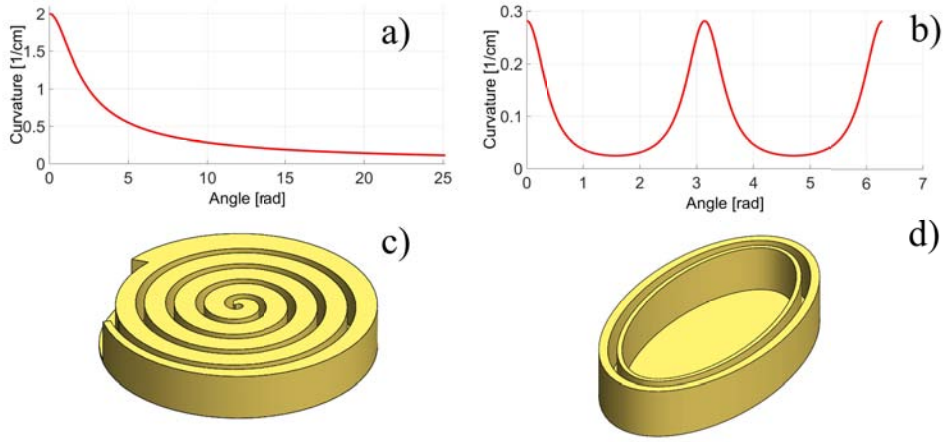

Figure 6: Curvature profiles inside spiral and ellipse are shown as functions of angle in a) and b). The spiral parameters are $a = 15$ cm and $b = 35$ cm. Parameters for ellipse are $a = 10$ cm and $b = 5$ cm. Standard polar equations for spiral and ellipse are used for calculations. Solid surface models of the shapes are given in c) and d). Curvature profiles are passing through midpoint of paths in both solid surface models.

A test platform composed of a soft actuator and sensor segment is undesirable. Pneumatic soft actuators typically possess relatively low bandwidth. Therefore, it constitutes a bottleneck for measuring dynamic responses of the sensor. Moreover, the magnet-Hall couple requires precise and repeatable calibration. Using soft actuators would introduce unnecessary complexity during the calibration phase.

To calibrate the sensor independent of external effects, and verify its static and dynamic response, we consider a custom test platform shown in Figure 5. Form-closed modular tracks that constrain the sensor segment to deform into exactly known curvature values are designed. The tracks can be rotated to desired angles or at desired velocities by a DC motor. A platform on top of the track holds the curvature sensor on a pin (see Figure 5), which pulls the sensor as the track advances.

The sensor needs to be deformed into known curvature values and kept at those values for calibration. For this task, we used an Archimedean spiral track and conduct static curvature tests. To verify accuracy and precision under dynamic curvature waveforms, we used an elliptical track. Figure 6 shows the spiral and ellipse plots along with their CAD models.

Curvature on any point on the spiral and the ellipse can be obtained by (4)

and (5) respectively. Here, a and b are standard ellipse and spiral parameters, $\theta \in [-\pi, \pi]$ is the angle of rotation around the center, and $t \in [-\pi, \pi]$ is a parametric variable for the ellipse, where $\tan(t) = (a/b)\tan(\theta)$. Simultaneous angle measurements were taken to calculate the expected curvature values during all experiments. The spiral track was used to collect data points for calibration, and for static response tests. Dynamic response tests were performed with the elliptical track.

$$\kappa_s = \frac{1}{\sqrt{a^2 + b^2 + b^2\theta^2 + 2ab}} \tag{4}$$

$$\kappa_e = \frac{ab}{\left[(b\cos t)^2 + (a\sin t)^2\right]^{3/2}} \tag{5}$$

A Maxon graphite brushed 200 W DC motor with 81:1 reduction was used for calibration. Accurate tracking was obtained with a 500 counts per turn optical encoder. Controller for this motor was programmed in an Arduino UNO board. Reference speed and angle values can be given to the controller through a user interface running on a PC through serial communication. PC-side user interface, and serial communication was programmed in Processing.

For speed tests, a 50 Watt motor with 19:1 reduction was used. An optical encoder with 64 counts per turn was used for tracking the angle. For analyzing the dynamic response of the sensor, the elliptical track was turned under different speeds in open loop, using a constant voltage input to the electric motor. Data from the soft curvature sensor and motor encoder was obtained through NI SCB-68A board. Sampling rate of data acquisition was 10 kHz.

Spiral and elliptical tracks are made of 3D printed ABS tracks. Initially, we performed tests with Ecoflex as the contact surface with the ABS tracks. This resulted in high friction. To overcome this issue we covered the sensor segment with 12.7 μm thick PET film and used industrial grease to further reduce friction.

3. Results and Discussion

In this section we are going to discuss our results from calibration, static loading and dynamic loading cases. We also give out characterization data of the proposed sensor design in Section 3.4.

3.1. Calibration

Based on simulations and previous experimentation with the sensor, the horizontal distance between the magnet and Hall element was set as 6 ± 0.5 mm. The vertical distance between the center of the magnet and the surface of the Hall element was dictated by the components to be approximately 0.2 mm. Horizontal and vertical distances can be seen in Figure 2. We also verified the static response of the curvature sensor using the test platform as a tool for automated calibration.

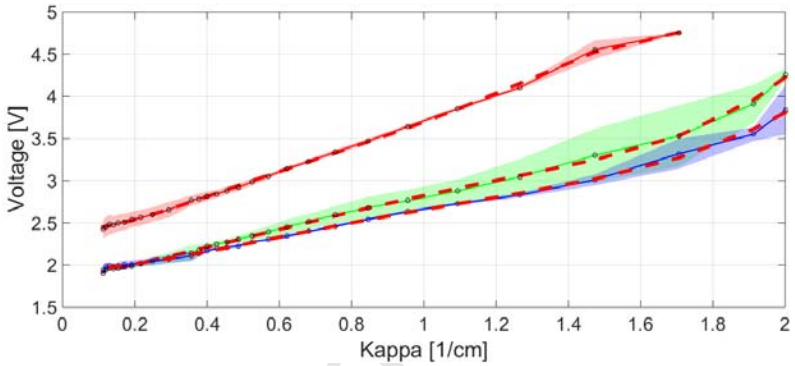

Figure 7: Calibration function obtained from data points inside a spiral. It shows change in voltage from 0.1 cm^{-1} to 2 cm^{-1}. Calibration is made for single direction. Three different voltage datasets are obtained from 30 different curvature points inside the spiral for three different sensors.

For automated calibration, sensor is driven to 30 points with different curvatures inside the spiral. This process was repeated three times for accuracy. A non-linear least squares fit was obtained between voltage and curvature values. A representative calibration fit for one of the tested sensors is shown in Figure 7. The calibration function is a third order polynomial with the following coefficients. $c_0 = 2.32$, $c_1 = 0.98$, $c_2 = 0.61$ and $c_3 = -0.20$.

Each sensor needs to be calibrated individually due to small manufacturing tolerances. Figure 7 shows mean and standard deviation of three calibration results from three sensors. Differences in magnet-sensor orientation and distance result in variations in calibration functions, although after a single initial calibration step, the curvature measurements are absolute. Results show that a precise positioning process would ensure repeatability.

3.2. Static Response

To verify the static response of a calibrated curvature sensor, we drove the sensor inside the spiral track. To show repeatability, we demonstrate results from two sensors. The calculated curvature inside the spiral is given in (4) and Figure 6 displays the curvature of the spiral track for a rotation angle range of $0\,^\circ - 1440\,^\circ$. A calibrated sensor is expected to follow a similar path. To this end, we drove sensors inside the spiral, with $5\,^\circ$ increments and waited 5 seconds at each curvature value for four full turns. Measured curvatures inside the spiral in comparison to expected values displayed in Figure 8 verify the ability of our sensor to measure curvatures accurately in a static setting.

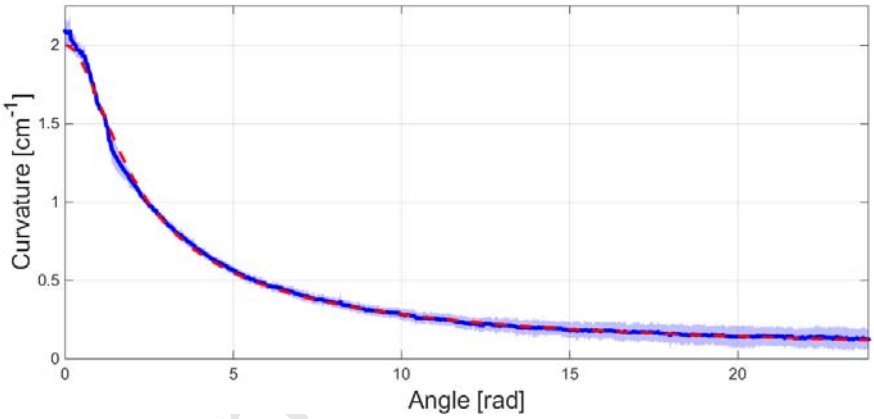

Figure 8: Static response of two different curvature sensors inside the spiral track using 5° increments. Each sensor was driven inside the spiral track three times. The dashed red curve is the actual curvature and the solid blue curve is the mean of measured curvatures. The shaded area displays the standard deviation of curvature measurements.

3.3. Dynamic Response

After verifying the ability of the proposed curvature sensors for static measurements, we tested the accuracy of its response under dynamic deformations. For speed tests, we used the elliptical track instead of a spiral. Just as the spiral track, walls of the ellipse controllably and repeatably deform the sensor into different and known curvature values, as a DC motor turns the platform, subjecting the sensor to a periodic curvature waveform.

A curvature sensor, moving inside the elliptical track is expected to register the periodic curvature changes continuously in a dynamic setting. A

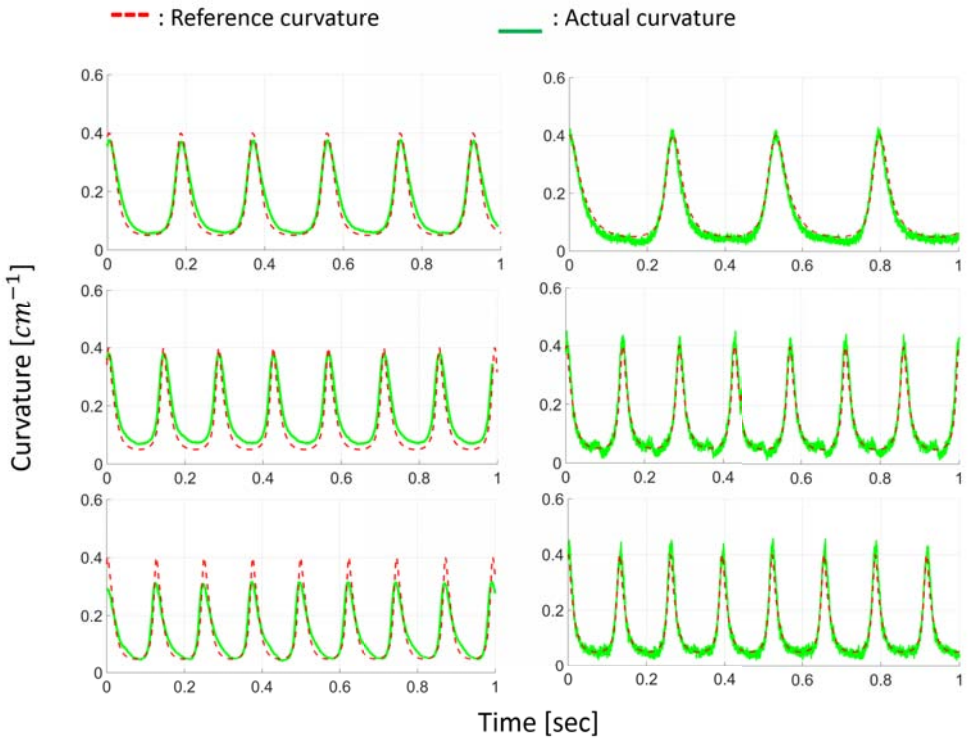

Figure 9: A close up of the sensor response for speed tests. Left column shows data obtained from sensor without low pass filter, right column shows response after the filter. Ellipse surface is turned at constant voltages of 8 V, 12 V, and 16 V, corresponding to average angular velocities of 11.6 rad/sec (3.69 Hz), 21.8 rad/sec (6.93 Hz), and 23.8 rad/sec (7.57 Hz) for the left column, and 16.9 rad/sec (5.37 Hz), 22 rad/sec (7.00 Hz) and 24.6 rad/sec (7.83 Hz) for the right column, from top to bottom.

detailed explanation of the elliptical shape and the curvature values can be seen in Figure 6. We drove the elliptical track under different input voltages resulting in different angular velocities. We collected angle information from the attached encoder and curvature information from the sensor itself, to compare measured and calculated curvature values. Using (5), angle data can be readily converted to calculate the expected curvature. Likewise, voltage information from the curvature sensor is passed through the calibration function to obtain measured curvature values. Raw curvature measurements are displayed in Figure 9 for two sensors in the elliptical track running at different velocities. These sensors represent two extremes: without any fil-

tering, and using a low-pass filter circuit with a very low cut-off frequency. Root mean square (RMS) errors of all dynamic tests can be seen in Table 1.

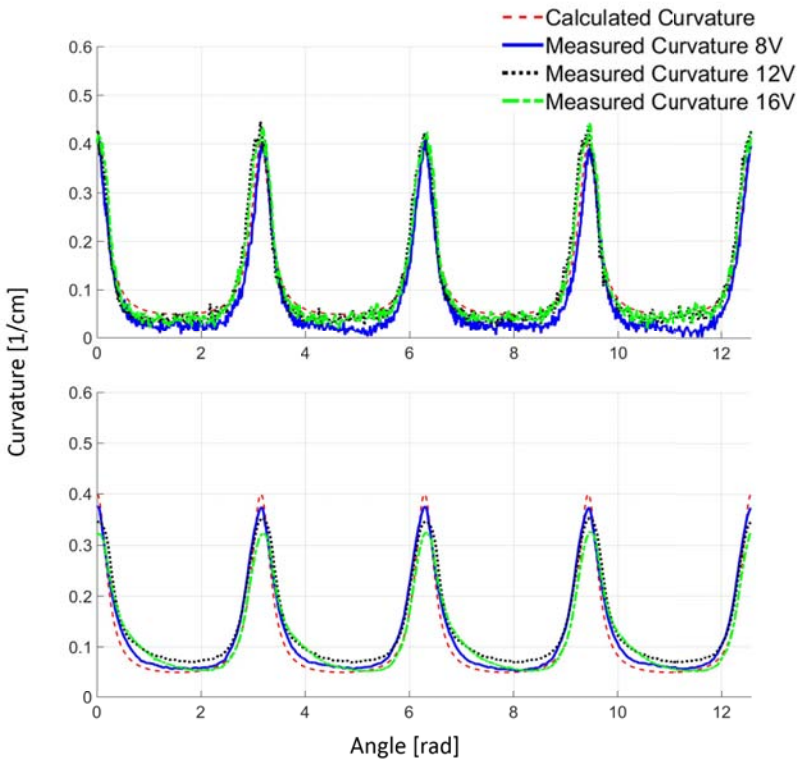

Figure 10: Measured and calculated curvature values are displayed with respect to the rotation angle of the elliptical track. Top panel shows data obtained from sensor without low pass filter; bottom panel shows response after the filter. The elliptical track was turned at constant voltages of 8 V, 12 V and 16 V. The corresponding angular velocities were 11.6 rad/sec (3.69 Hz), 21.8 rad/sec (6.93 Hz) and 23.8 rad/sec (7.57 Hz) for top panel, and 16.9 rad/sec (5.37 Hz), 22 rad/sec (7.00 Hz) and 24.6 rad/sec (7.83 Hz) bottom panel.

High noise can be observed in the left panel of Figure 9. The low-pass filter attached to the output channel reduces noise, as shown in the right panel of Figure 9. We used 3.2 Hz as cutoff frequency to study its effect on the dynamic response. Filtered sensor was successful in yielding reduced noise, at the expense of an attenuated response to higher frequency deformations. A lagged behavior can be observed in the right column of Figure 9. As expected, when the sensor is deformed faster, it is not able to settle on the calculated

curvature values. Thus, a low pass filter with an appropriate cutoff frequency is required. Our intended application, the soft snake robot undulates at frequencies up to 2 Hz and our choice of 3.2 Hz cutoff is sufficient. Measured curvature versus angle of the ellipse results are given in Figure 10. When the low-pass filter is used for noise cancellation, a deterioration in peak to peak difference is observed. The peak-to-peak amplitude response of both sensors with noise cancellation to bending under different frequencies is displayed in Figure 11.

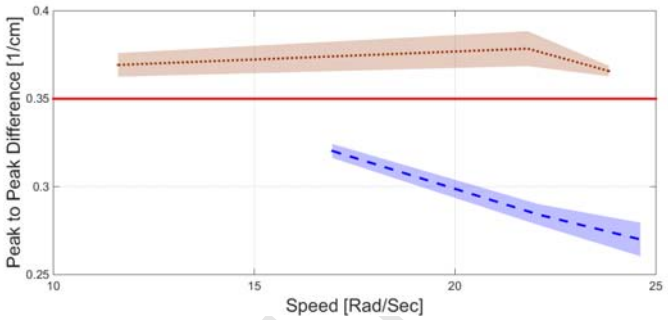

Figure 11: Peak-to-peak curvature responses of each sensor in Figure 10 is given along with calculated peak-to-peak response from ellipse surface. Overshoot in the sensor without filter (dot) and decay in filtered sensor (dash) due to delay can be observed. Variance of peak to peak curvature responses are indicated as shaded areas.

In addition to verifying the measurement capability of the proposed curvature sensors, experimental studies also informed us with details on manufacturing requirements. For example accurate and repeatable positioning of the magnet and Hall element pair is crucial for obtaining the expected calibration function, since the curvature response due to magnetic field measurements is very sensitive in the proposed arrangement. However, we have shown that, even for manual fabrication, a monotonically increasing, one-to-one mapping function exists.

During dynamic bending experiments, we determined that among the two substrates, copper-clad FR4 sheets exhibited reduced strength. For periodic loading of curvature waves, the chemically bonded copper traces eventually failed due to bending stresses and fatigue, especially for larger frequencies in Figure 9. However, copper foil tape laminated on polyester (PET) films exhibited improved endurance to this failure mode (the first curvature sensor made using this substrate is still functional), since the flexible adhesive

	With Filter	Without Filter
8 V	0.021	0.026
12 V	0.037	0.023
16 V	0.030	0.024

Table 1: Root mean square errors between measured and reference curvature data from Figure 9. Unit of measurement is cm^{-1}. The elliptical platform is driven in open loop with three different constant voltage values: 8 V, 12 V and 16 V.

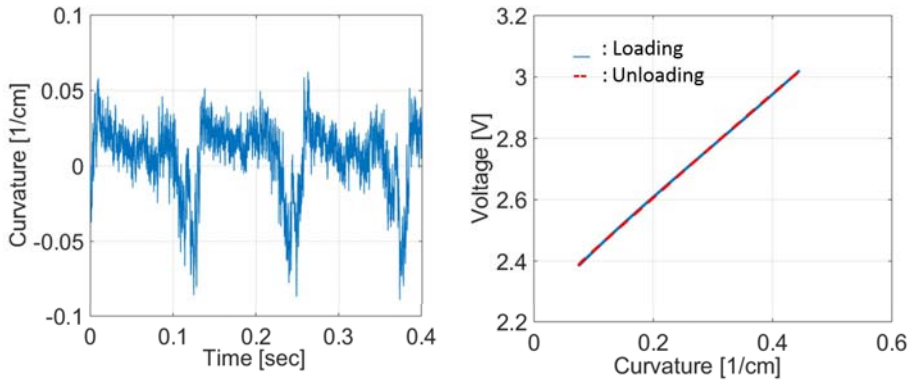

Figure 12: Left: Error between reference curvature and measured curvature when elliptical track is turned with an angular velocity of 23.8 rad/sec. No filtering is applied. Right: Relationship between voltage and curvature when curvature is bent from 0.05 cm^{-1} to 0.45 cm^{-1} and back to 0.05 cm^{-1}. No hysteresis is detected.

layer can deform and absorb the bending stresses. Thus, all dynamic tests were performed on curvature sensors printed on copper foil laminated PET substrates for reliability.

3.4. Discussion

Hysteresis, linearity and accuracy of the sensor is shown in Figure 12. We detected no hysteresis when elliptical track was rotated at different speeds. A linear relationship between voltage output from the sensor and curvature is also observed in the right panel in Figure 12. The root mean square for the error signal between the actual curvature and reference curvature is 0.0239 cm^{-1}. The slope of a linear fit on the curve in Figure 12 is 0.00056 cm^{-1}/mV. This suggests that curvatures as small as 0.0012 cm^{-1} can be measured using a 12 bit digital-to-analog converter. In reality, that

level of accuracy cannot be achieved without reducing the noise in the sensor. During the speed tests for dynamic loading, the maximum peak to peak value of intrinsic noise without filtering was measured as 0.05 cm^{-1}, which also represents the minimum detectable curvature in our current settings without filtering.

4. Conclusion

In this paper, we presented a novel soft curvature sensor concept and tested it rigorously. The soft sensor is specifically designed to be used with a soft snake for measuring curvatures, although it can be adapted to measuring various deformations in soft bodies through minor modifications.

The proposed curvature sensor system can be built on assembly lines. Consecutive phases in manufacturing, such as printing circuit traces, etching, populating components, and molding silicone rubber can be connected by basic pick-and-place operations. We also discovered that hand calibrating each sensor using a calibration ruler is prone to human error and requires a skilled individual for accurate calibration. For an automated calibration phase as well as repeatable dynamic testing of curvature sensors, we described a custom test platform using continuously changing form-closed tracks.

We demonstrated the accuracy of the sensor under dynamic loading. Results suggest that the proposed sensors are accurate and reliable. They can be used for reconstructing configuration for control applications that require accurate sensing.

The same idea behind our sensing modality can be adapted to measuring different physical quantities, such as force applied on a soft structure as a function of distance. Our current work considers single axis, soft-bodied force sensors. A potential future work is to apply this sensing platform to human health monitoring.

[1] P. Taylor, D. Trivedi, C. D. Rahn, W. M. Kier, I. D. Walker, Soft robotics: Biological inspiration, state of the art, and future research (2008).

[2] F. Saunders, E. Golden, R. D. White, J. Rife, Experimental verification of soft-robot gaits evolved using a lumped dynamic model, Robotica 29 (2011) 823–830.

[3] F. Ilievski, A. D. Mazzeo, R. F. Shepherd, X. Chen, G. M. Whitesides, Soft robotics for chemists, Angewandte Chemie 50 (2011) 1890–1895.

[4] M. Luo, M. Agheli, C. D. Onal, Theoretical modeling and experimental analysis of a pressure-operated soft robotic snake, Soft Robotics (2).

[5] M. Cianchetti, A. Arienti, M. Follador, B. Mazzolai, P. Dario, C. Laschi, Design concept and validation of a robotic arm inspired by the octopus, Materials Science and Engineering: C 31 (6) (2011) 1230 – 1239, principles and Development of Bio-Inspired Materials.

[6] A. Marchese, K. Komorowski, C. Onal, D. Rus, Design and control of a soft and continuously deformable 2d robotic manipulation system, in: Robotics and Automation (ICRA), 2014 IEEE International Conference on, 2014, pp. 2189–2196.

[7] R. F. Shepherd, F. Ilievski, W. Choi, S. A. Morin, A. A. Stokes, A. D. Mazzeo, X. Chen, M. Wang, G. M. Whitesides, Multigait soft robot, Proceedings of the National Academy of Sciences 108 (51) (2011) 20400–20403.

[8] H.-T. Lin, G. G. Leisk, B. Trimmer, Goqbot: a caterpillar-inspired soft-bodied rolling robot, Bioinspiration and Biomimetics 6 (2).

[9] M. Tolley, R. F. Shepherd, M. Bobak, K. C. Galloway, M. Wehner, M. Karpelson, R. J. Wood, G. M. Whitesides, A resilient, untethered soft robot, Soft Robotics 1 (3) (2014) 213–223.

[10] C. D. Onal, D. Rus, Autonomous undulatory serpentine locomotion utilizing body dynamics of a fluidic soft robot, Bioinspiration & biomimetics 8 (2) (2013) 026003.

[11] A. D. Marchese, R. K. Katzschmann, D. Rus, Whole arm planning for a soft and highly compliant 2d robotic manipulator, in: Intelligent Robots and Systems (IROS), 2014 IEEE/RSJ International Conference on.

[12] M. Luo, M. Agheli, C. D. Onal, Theoretical modeling and experimental analysis of a pressure-operated soft robotic snake, Soft Robotics 1 (2).

[13] J. Butterfass, M. Grebenstein, H. Liu, G. Hirzinger, Dlr-hand ii: next generation of a dextrous robot hand, in: Robotics and Automation, 2001. Proceedings 2001 ICRA. IEEE International Conference on, Vol. 1, 2001, pp. 109–114 vol.1.

[14] A. Dollar, R. Howe, A robust compliant grasper via shape deposition manufacturing, Mechatronics, IEEE/ASME Transactions on 11 (2) (2006) 154–161. doi:10.1109/TMECH.2006.871090.

[15] T. J. Eduardo, I. Vasilescu, R. Coral, A soft touch: Compliant tactile sensors for sensitive manipulation (2003).

[16] L. Jamone, L. Natale, G. Metta, G. Sandini, Highly sensitive soft tactile sensors for an anthropomorphic robotic hand, Sensors Journal, IEEE PP (99) (2015) 1–1. doi:10.1109/JSEN.2015.2417759.

[17] D. M. Karol, P.-C. Ramon, D. Floreano, Contactless deflection sensor for soft robots, in: International Conference on Intelligent Robots and Systems, 2011.

[18] Y.-L. Park, K. Chau, R. Black, M. Cutkosky, Force sensing robot fingers using embedded fiber bragg grating sensors and shape deposition manufacturing, in: Robotics and Automation, 2007 IEEE International Conference on, 2007, pp. 1510–1516.

[19] J. Yi, X. Zhu, L. Shen, B. Sun, L. Jiang, An orthogonal curvature fiber bragg grating sensor array for shape reconstruction, in: K. Li, X. Li, S. Ma, G. Irwin (Eds.), Life System Modeling and Intelligent Computing, Vol. 97 of Communications in Computer and Information Science, Springer Berlin Heidelberg, 2010, pp. 25–31.

[20] H. E. Holling, H. C. Boland, E. Russ, Investigation of arterial obstruction using a mercury-in-rubber strain gauge 62 (2) (1961) 194–205.

[21] R. Kramer, C. Majidi, R. Sahai, R. Wood, Soft curvature sensors for joint angle proprioception, in: Intelligent Robots and Systems (IROS), 2011 IEEE/RSJ International Conference on, 2011, pp. 1919–1926.

[22] R. Kramer, C. Majidi, R. Wood, Wearable tactile keypad with stretchable artificial skin, in: Robotics and Automation (ICRA), 2011 IEEE International Conference on, 2011, pp. 1103–1107.

[23] D. Vogt, Y. Mengus, M. Y.-L Park, R. K. Kramer, C. Majidi, L. P. Jentoft, R. D. H. Y. Tenzer, R. J. Wood, Progress in soft, flexible, and stretchable sensing systems, in: International Conference on Robotics and Automation (ICRA), 2013 IEEE/RSJ International Conference on, 2013.

[24] Y. Menguc, Y.-L. Park, H. Pei, D. Vogt, P. Aubin, E. Winchell, L. Fluke, L. Stirling, R. Wood, C. Walsh, Wearable soft sensing suit for human gait measurement, International Journal of Robotics Research.

[25] E. P. Furlani, Chapter 4 - permanent magnet applications, in: E. P. Furlani (Ed.), Permanent Magnet and Electromechanical Devices, Electromagnetism, Academic Press, San Diego, 2001, pp. 207 – 333.

[26] M. Luo, W. Tao, F. Chen, T. Khuu, S. Ozel, C. Onal, Design improvements and dynamic characterization on fluidic elastomer actuators for a soft robotic snake, in: Technologies for Practical Robot Applications (TePRA), 2014 IEEE International Conference on, 2014, pp. 1–6.

Highlights

- Robust and precise curvature feedback with rapid response for soft-bodied robots.
- Integrated measurement of kinematic configuration for soft-bodied arms and mobile robots composed of soft bending segments.
- A custom test platform for soft-bodied curvature sensors.

Selim Ozel

Selim Ozel is a second year PhD student in Robotics Engineering Program at Worcester Polytechnic Institute. His interest in robotics started during freshman year in college. Later on, he received B.Sc and M.Sc degrees in Mechatronics Engineering from Sabanci University, Turkey, in 2011 and 2013. His B.Sc thesis was on stable center of mass trajectory generation for legged robots. As for his M.Sc thesis, he worked on action estimation for robot manipulators. His current research is on sensorization of soft bodied materials, soft robotics, control theory and legged locomotion.

Nehir Keskin

Upon completing her secondary education in Turkey, Nehir Keskin received her BS degree in mechanical engineering from Worcester Polytechnic Institute in 2015. During her undergraduate degree she focused on mechanical design and rapid prototyping integration in engineering. Nehir successfully completed her senior capstone project working on the design and production of a 3D-printed wireless hexapod. Along with design, she has interest in renewable energy and biomechanics. She currently works as a CAD Engineer in the field of biomechanics, and she plans on pursuing graduate education in the field of sustainable energy technologies.

Darien Khea

I'm currently pursuing a Bachelor of Science degree in mechanical engineering. My interest in research and development was what lead me to become affiliated with the Soft Robotics Lab. I decided to pursue this project because I believe that sensors play an important role in the constant advancements in technology. Because they offer a wide range of benefits, soft bodied robots are gaining more recognition today. These benefits include the ability of these robots to be implemented in biomedical applications as well as the assistance of these robots in disastrous events. Apart from this research, I am developing an algorithm for torque vectoring in cars. In addition, I am assisting in institutional research in the field of electric propulsion.

Cagdas Onal

Cagdas D. Onal is an Assistant Professor of Mechanical Engineering and Robotics Engineering at WPI. He received the B.Sc. and M.Sc. degrees from Mechatronics Engineering Program, Sabanci University, Turkey, in 2003 and 2005, respectively; and the Ph.D. degree in Mechanical Engineering from Carnegie Mellon University, in 2009. He was a Postdoctoral Associate in the Computer Science and Artificial Intelligence Laboratory, MIT. Onal is the co-author of a textbook on Nanorobotics. His current research interests include soft robotics, printable robotics, alternative actuation/sensing mechanisms, bio-inspiration, control theory, and micro/nano-science and technology.